

# MAESTROCUT: A Closed-Loop Framework for Dynamic, Noise-Adaptive and Cryptographically Secure Quantum Circuit Cutting on Near-Term Hardware

Samuel Punch  
School of Computer Science  
University College Cork  
Cork, Ireland  
samuel.punch@ucc.ie

Krishnendu Guha  
School of Computer Science  
University College Cork  
Cork, Ireland  
k.guha@ucc.ie

**Abstract**—We present MAESTROCUT, a *closed-loop* framework for quantum circuit cutting that makes large circuits practical on NISQ hardware by operating on adaptive fragments rather than fixed, one-shot cuts. MAESTROCUT comprises four co-designed modules that update online: an incremental multilevel-FM partitioner, a topology-aware Gaussian-process shot allocator (*Topo-GP*), an entropy-gated estimator cascade that switches between classical-shadows and MLE, and a Pauli-compatible confidentiality layer (PHASEPAD-OTP) with IND-CFA security at  $\approx 1\%$  runtime overhead. The system targets scalable, drift-resilient, and confidential execution while respecting end-to-end SLOs.

Circuit cutting at scale is impeded by four intertwined issues: (i) exponential sampling overhead from entangling cuts, (ii) time-varying device drift invalidating static calibrations, (iii) topology-agnostic allocation that wastes shots on correlated errors, and (iv) plaintext fragment exposure to semi-honest providers. Static plans and offline calibrations are brittle under queue and noise fluctuations; conversely, heavyweight privacy can jeopardize latency/throughput budgets. MAESTROCUT addresses these tensions by coupling drift tracking with topology-aware reallocation and by enforcing confidentiality that is compatible with Pauli pipelines and estimator choice.

We close the loop with Kalman tracking and CUSUM triggers for repartition, water-filling over a heavy-hex correlation proxy (Topo-GP), and an entropy/shot-aware cascade. In Tier-1 simulation (five workloads, shared seeds), this reduces variance relative to uniform allocation and suppresses heavy shot tails while aligning cascade decisions with the predicted  $H$ - $s$  boundary. In Tier-2 emulation under calibrated Baseline/Noisy/Bursty/Adversarial scenarios, jitter remains well within target ( $\leq 150$  ms; medians 29/43/101/45 ms); time-to-first-result meets the 220 ms target except under *Noisy* (+1 ms) and *Adversarial* (+26 ms) contention (medians 169/221/169/246 ms); reliability stays within caps (success 100/100/99.75/98%, timeouts 0/0/0.25/0%, errors 0/0/0/2%); and throughput degrades smoothly without tail amplification (46.4k/42.6k/41.4k/43.4k QPS). PHASEPAD-OTP preserves end-to-end performance at the 1% setting (relative throughput  $\approx 98$ –99%), providing confidentiality with near-free system cost. Together, these results demonstrate adaptive, topology-aware cutting with auditable overheads suitable for NISQ-era deployments.

**Index Terms**—quantum circuit cutting, dynamic partitioning, drift-aware shot allocation, estimator cascade

## I. INTRODUCTION

*Circuit cutting* lets NISQ hardware execute problems that exceed on-chip qubit counts by running fragments and classically reconstructing global observables. However, practical deployment faces coupled systems challenges: sampling blow-up from cuts, time-varying noise and queue drift, topology heterogeneity, and provider visibility into fragment structure and measurement strings. These factors limit scalability, distort error budgets, and expose sensitive algorithm information even when final outputs are correct. **We ask: how can cutting be made deployable under live drift while preserving fragment confidentiality and end-to-end budgets? Our answer is MAESTROCUT, a closed-loop co-design that adapts partitioning, allocation, and estimation while enforcing security and audit policies, with evidence from Tier-1 simulation and Tier-2 emulation.**

*Challenges:* Deployable cutting on shared back ends must:

- (i) control sampling overhead at run time under  $\mu$ s-scale control loops and minute-scale drift,
- (ii) adapt partitioning to heterogeneous heavy-hex topologies and changing error profiles,
- (iii) allocate shots online with provable variance contraction and budget compliance (see Section IV for the bound),
- (iv) preserve confidentiality of fragments and operational metadata with auditable abort semantics,
- (v) meet latency, memory, and energy constraints across QPU, TN, CPU, and GPU targets.

*Prior work and limitations:* Point solutions typically address a single axis in isolation. *Overhead/topology:* offline or static partitioners reduce e-bits but assume frozen calibrations [1], [2]. *Estimation:* contraction and stabilising estimators improve robustness but ignore shot routing [3], [4]. *Allocation:* ShotQC variants reduce variance yet are commonly tuned offline [5], [6]. *Privacy/metadata:* blind-compute protocols hide algorithm content but are rarely integrated with cutting or estimator choice [7], while recent work shows link and scheduler metadata can leak work profiles [8]. As a result,

partitioning, allocation, estimator selection, and confidentiality are not co-optimised in a closed loop.

*Motivating example:* A tenant must choose between two cut strategies with e-bit counts  $e_1 < e_2$ . Under a transient hot-spot on a heavy-hex pair, the lower- $e$  option yields higher variance due to local readout drift. A static plan overspends shots on the degraded region and leaks work profile through shot vectors. In contrast, our monitor observes features derived from queue and calibration deltas, *re-partitions* to reduce exposure, and re-allocates shots via a Kalman-updated plan; if an online leakage or variance budget is exceeded, execution aborts and the event is immutably logged (see Figure 1 and Figure 2).

*Our work (MAESTROCut):* MAESTROCut is a closed-loop co-design that enforces end-to-end budgets while adapting to drift and topology in real time:

- **Maestro-Partition.** Incremental multilevel-FM hypergraph partitioning that re-cuts under drift to minimise e-bits while respecting device topology.
- **ShotQC-Kalman with Topo-GP.** Online variance tracking with Kalman updates and Gaussian-process priors over heavy-hex error landscapes for shot allocation.
- **Estimator Cascade.** An entropy-gated switch among de-randomised shadows, twirled maximum-likelihood, and MCMC-based contraction for stable post-processing.
- **PhasePad-OTP.** Pauli-compatible padding with the quantum one-time pad (QOTP) and authenticated encryption with associated data (AEAD), plus decoy tests and an auditable kill-switch; security goal is indistinguishability under chosen-fragment attack (IND-CFA).
- **Hybrid execution.** A backend-agnostic path that routes Clifford-heavy fragments to TN/CPU/GPU while reserving non-Clifford fragments for the QPU.

*Contributions:*

- **Metric and policy.** Online variance and leakage budgets with abort semantics and immutable audit events that compose across partitioning, allocation, and estimation.
- **Orchestration.** A practical pipeline coupling Maestro-Partition, ShotQC-Kalman with Topo-GP, PhasePad-OTP, and a monitored kill-switch (procedure in Section IV; overview in Figure 1).
- **Security layer.** A threat model and Universal-Composability (UC)-style games for confidentiality, verifiability, and availability with Local-Shadow checks and shot-vector privacy (Section III; Figure 2). For clarity, *blind compute* denotes interactive protocols (e.g., UBQC), whereas *fragment encryption* denotes non-interactive Pauli padding applied to cut fragments.
- **Evidence—Tier-1.** Simulation across representative workloads shows variance contraction versus uniform allocation, suppression of heavy shot tails, and estimator choices that align with the predicted entropy/shot decision boundary.
- **Evidence—Tier-2.** Emulation under calibrated noise and queue dynamics demonstrates stable short-term latencies (jitter), satisfaction of reliability caps, smooth throughput

degradation under stress without tail amplification, and preservation of system SLOs when confidentiality is enabled; sensitivity appears only in first-result latency (*time-to-first-result*, TTFR) under adversarial queueing.

- **Evaluation scope.** Claims are substantiated with Tier-1 and Tier-2; *Tier-3 hardware runs are in progress and are not used to support deployability claims in this version.*

*Paper organisation:* Section II reviews circuit cutting, allocation, estimators, and confidentiality. Section III states the system and threat model. Section IV details partitioning, allocation, estimators, and orchestration. Section V reports Tier-1 and Tier-2 results, with Section VI discussing limitations and outlook.

## II. BACKGROUND AND MOTIVATION

Circuit cutting decomposes monolithic quantum circuits into sub-circuits executable on noisy-intermediate-scale (NISQ) hardware, trading *quantum depth* for *classical post-processing*. Foundational baselines—**wire cutting** [9] and **CutQC** [10]—established the core cluster/fragment model and practical stitching under NISQ constraints. While enabling VQE/QAOA instances beyond device limits, four systemic obstacles persist:

- 1) **Sampling overhead**—With  $e$  wire-cuts, naïve cost scales as  $\mathcal{O}(2^e)$ . **For six cuts, this implies 64 settings and  $>10^6$  shots on superconducting hardware.** Partial solutions each target a single factor: non-maximally entangled cuts ( $\approx 1.6^e$ ) [11]; ILP-guided QRCC removes **29%** of cuts on BV-102 and  $\approx 43\%$  on random-QAOA-48 [12]; ShotQC reduces *stitched-variance / sampling overhead* by up to **19 $\times$**  on evaluated benchmarks [5]; basis-element neglect ( $(1.5-1.7)^e$  in small demos) [13]; QCS-Shadows lowers samples for high-weight observables [14]; *randomised-measurement cutting* achieves  $\tilde{O}(4^k/\varepsilon^2)$  sample overhead for  $k$  parallel wire-cuts and proves an information-theoretic lower bound  $\Omega(2^k/\varepsilon^2)$ ; demonstrated on structured QAOA instances [1]; pruning yields **16 $\times$**  fewer settings [15]; Metropolis reconstruction runs linearly for  $\leq 2$  cuts [2]. None handle drift or confidentiality.
- 2) **Time-dependent drift**—Hour-scale swings in  $T_1/T_2$ , read-out error, and crosstalk invalidate daily calibrations.
- 3) **Topology blindness**—Uniform shot budgets ignore heavy-hex error landscapes, wasting effort on correlated pairs. *FragQC* boosts fidelity by  $\approx 14.8\%$  on IBM hardware but remains offline and shot-agnostic [6].
- 4) **Provider visibility**—Raw fragments leak intellectual property. We target *confidential execution* (fragment/metadata secrecy) via the Pauli one-time pad (QOTP): encrypting an  $n$ -qubit fragment *requires and suffices with  $2n$  uniformly random key bits* for information-theoretic secrecy; this bound is optimal. A restricted special case—*real-amplitude product states*—can be hidden with  $n$  bits; we do not rely on this case [16]. QOTP provides confidentiality only (no authentication/integrity). By contrast, *blind-compute* protocols such as UBQC achieve blindness through *interactive* MBQC with client-prepared random single-qubit states,

TABLE I  
CORE FRAMEWORKS. A TICK (✓) INDICATES THE WORK PRIMARILY ADDRESSES THAT AXIS. OVERHEAD = REDUCES SAMPLING VARIANCE/SHOT COMPLEXITY OR REDUCES CUT COUNT/SETTINGS. A DASH (—) DENOTES NOT APPLICABLE (NON-FRAGMENTATION).

| Framework                       | Overhead | Drift | Topo. | Priv. |
|---------------------------------|----------|-------|-------|-------|
| WireCut (Peng’20) [9]           | ✗        | ✗     | ✗     | ✗     |
| CutQC (ASPLOS’21) [10]          | ✓        | ✗     | ✓     | ✗     |
| FastCut (Lowe’23) [1]           | ✓        | ✗     | ✗     | ✗     |
| MLEcut / MLFT (Perlin’21) [18]  | ✗        | ✗     | ✗     | ✗     |
| ShotQC (Chen’24) [5]            | ✓        | ✗     | ✗     | ✗     |
| QCS-Shadows (Chen’24) [14]      | ✓        | ✗     | ✗     | ✗     |
| QRCC (Pawar’24) [12]            | ✓        | ✗     | ✓     | ✗     |
| MLFM (Burt’25) [19]             | ✓        | ✗     | ✓     | ✗     |
| Adaptive-PEC (Dasgupta’23) [20] | —        | ✓     | ✗     | ✗     |
| CaliScalpel (Fang’24) [21]      | —        | ✓     | ✗     | ✗     |
| <b>MaestroCut (this work)</b>   | ✓        | ✓     | ✓     | ✓     |

hiding the computation up to unavoidable size leakage; these are orthogonal to our *non-interactive* encrypted-fragment setting [17]. Recent cloud timing/metadata side-channels further motivate fragment/metadata hardening [8]; ancilla-driven verification [4] does not integrate cutting.

**Table I summarises core frameworks across Overhead, Drift, Topology, and non-interactive fragment confidentiality.**

*Complementary knitting.*: Complementing pure cutting, *circuit knitting with classical communication* can provably reduce sampling overhead—for  $n$  nonlocal CNOTs from  $O(9^n)$  to  $O(4^n)$ —and gives closed-form  $\gamma$ -factors for many Clifford and controlled-rotation gates; in other gate families, classical communication yields no advantage. These CC-optimal schemes remain static and noise-blind, contrasting with our runtime drift-tracking and confidentiality aims [22].

*Key prior work.*: **Multilevel-FM** [19] reduces e-bits by 33% but assumes frozen calibrations and plaintext data; we add drift awareness and PhasePad-OTP. **BasisNeglect** [13] drops zero-weight Pauli terms  $((1.5-1.7)^e$  in small demos), orthogonal to our drift-aware allocation and privacy. **QCS-Shadows** [14] follows the HKP classical-shadows framework [23], reducing sample complexity but remaining noise-blind and non-private. **ShotQC** [5] achieves up to  $19\times$  overhead reduction but lacks continuous drift tracking and privacy. **Perlin (MLFT)** [18] provides a maximum-likelihood stitching baseline that enforces a valid probability distribution and can outperform direct execution under fixed shot budgets. **Lowe et al.** [1] use randomised measurements to cut wires with  $\tilde{O}(4^k/\epsilon^2)$  samples and prove an  $\Omega(2^k/\epsilon^2)$  lower bound; effective on QAOA-like structure. **Chen (MCMC)** [2] approximates reconstruction tensors linearly for  $\leq 2$  cuts; complementary but not partition-optimised. **Li et al.** [15] exploit sparsity but ignore noise drift and confidentiality. **NMECS** [11] lowers per-cut sampling by  $1.6\times$  without addressing key limitations. **QRCC** [12] removes **29–43%** of cuts but lacks dynamic adaptation. **UBQC** [17] and **ADBQC** [4] enable verification-centric privacy via interactive MBQC with size leakage; MaestroCut targets *operational* fragment/metadata confidentiality in a non-interactive setting,

strengthened by QOTP ( $2n$  key bits, optimal) [16] and motivated by cloud leaks [8].

**No prior framework co-optimises all four axes.** MAESTRO-CUT closes this gap with a cloud-ready, closed-loop stack that dynamically repartitions circuits, reallocates shots under drift, switches estimators on entropy cues, and encrypts fragments via PhasePad-OTP—delivering scalable, drift-resilient, topology-aware confidential distributed quantum computation.

### III. THREAT MODEL & SECURITY LAYER

This section first outlines the MAESTRO-CUT system architecture and run-time orchestration (Figure 1), then states the threat model, adversary classes, and the security layer with mitigations (Figure 2).

#### A. System Overview

Figure 1 shows the end-to-end pipeline.

*Modules and flow.*:

- **Circuit & policy.** The client provides a circuit and policy budgets (variance and leakage).
- **Compiler (Qiskit/tket).** Produces an IR that respects device constraints.
- **Maestro-Partition.** Incremental multilevel-FM hypergraph partitioning; emits fragments  $F_i$  while tracking e-bits and cut cost.
- **PhasePad-OTP.** Pauli-compatible padding and encryption of fragments with lightweight decoys for integrity checks.
- **ShotQC (Kalman) + Topology-GP.** Online shot allocation using Kalman-updated variance estimates and Gaussian-process priors over heavy-hex error landscapes.
- **Back-end.** Hybrid execution across QPU / TN / CPU / GPU targets as appropriate.
- **Monitor & kill-switch.** Observes queue and calibration deltas and enforces policy budgets; aborts on violations and logs the event immutably.
- **Results & proofs.** Decrypt & stitch returns observables with audit evidence.

*Feedback.*: Two run-time feedback paths (Figure 1) ensure adaptivity: (i) leakage feedback into PhasePad to adjust padding and decoys, and (ii) variance updates into ShotQC for budget-respecting reallocation.

## MAESTROCut System Overview

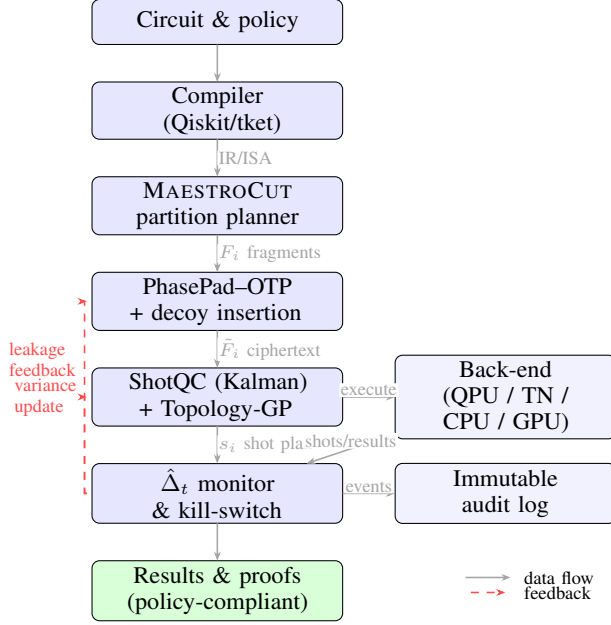


Fig. 1. System pipeline for MAESTROCut: policy-aware compilation, circuit cutting and phase padding, adaptive shot allocation, monitored execution with leakage-bound enforcement, and immutable audit logging.

## MAESTROCut Threat Model

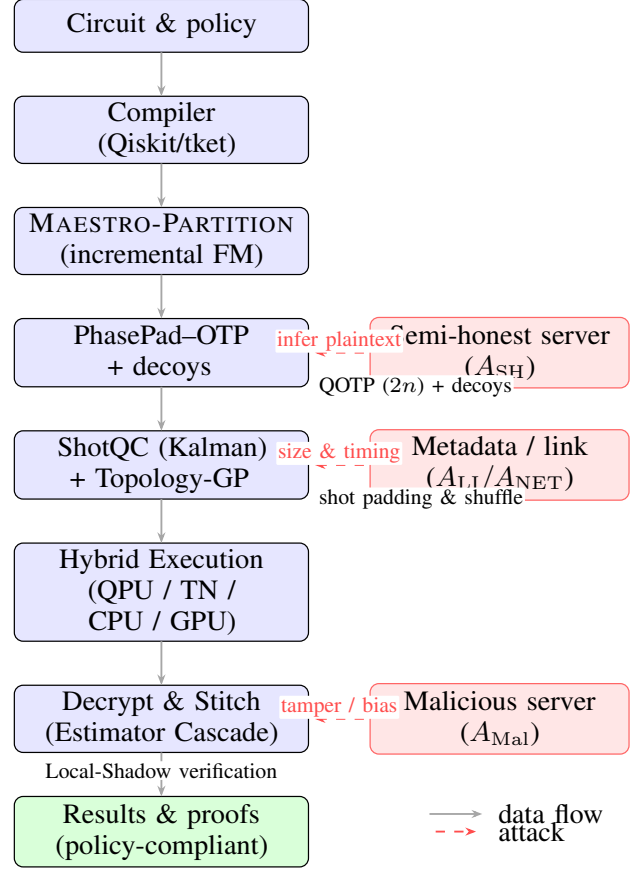


Fig. 2. Threat model over the MAESTROCut pipeline. Red boxes denote adversaries; dashed arrows indicate attack surfaces; inline labels show primary mitigations.

### B. Threat Model & Security Layer

We assume a trusted client  $\mathcal{C}$  and post-processor  $\mathcal{P}$ , and an execution provider  $\mathcal{S}$  that is *semi-honest* for confidentiality (may inspect traffic and metadata) and *potentially malicious* for integrity and availability. The protected assets include ciphertext fragments  $\tilde{F}_i$ , shot vectors  $s_i$ , outcomes, keys, topology/error priors, and the audit log. The security objectives are: (i) confidentiality of fragments and shot vectors, (ii) integrity and verifiability of stitched results, and (iii) availability within stated service bounds. Figure 2 maps adversaries to the pipeline and shows the primary mitigations at each locus.

| Objective                             | Primary Mitigation                               | Evidence                     |
|---------------------------------------|--|------------------------------|
| Confidentiality of $\tilde{F}_i, s_i$ | PhasePad-OTP <sup>1</sup> ; shot padding/shuffle | Sec. IV; Tier-2 budget       |
| Integrity & verifiability             | Decoys; Local-Shadow checks; abort & re-key      | Sec. IV; Sec. V-D            |
| Availability within SLOs              | Fixed-rate sends; budgeted decoys; kill switch   | Tier-2 latency / reliability |

<sup>1</sup>Quantum One-Time Pad + Authenticated Encryption with Associated Data.

#### Participants and trust boundaries.:

- **Client ( $\mathcal{C}$ ).** Generates and rotates  $K_{\text{mast}}$  per fragment batch; performs PhasePad encryption and post-decrypt Local-Shadow checks.
- **Provider ( $\mathcal{S}$ ).** Executes  $\text{Execute}(\tilde{F}_i, s_i)$ ; returns ciphertext outcomes with calibration metadata.
- **Post-processor ( $\mathcal{P}$ ).** Trusted: decrypts, verifies decoys, stitches, and emits auditable results.

#### Adversary classes and mitigations.:

- $A_{\text{SH}}$  (semi-honest provider): attempts to infer plaintext fragments. *Mitigation:* PhasePad-OTP with decoys.
- $A_{\text{Mal}}$  (malicious provider): tampers with fragments or outcomes. *Mitigation:* decoy/trap checks, Local-Shadow verification, abort & re-key.
- $A_{\text{SV}}$  (shot-vector inference): infers work profile from  $s_i$ . *Mitigation:* shot padding and shuffling; parameter randomisation.
- $A_{\text{LI}} / A_{\text{NET}}$  (link/metadata observers): exploits sizes, rates, and timing. *Mitigation:* AEAD padding, uniform packet padding, fixed-rate sends; optional onion routing.

- **A<sub>SC</sub>** (supply-chain): compiler/firmware back-doors. *Mitigation*: client-side transpilation, reproducible builds, TPM-backed attestation, binary differencing.
- **Physical side-channels** (EM/acoustic): treated as out-of-scope; timing obfuscation and vendor shielding assumed.

*Residual risks (metadata)*.: PhasePad hides plaintext fragments and measurement strings; however, under our semi-honest provider and link observer model, the following coarse signals may remain:

- *Envelope size bins*: AEAD padding equalises packet formats but may reveal coarse size buckets.
- *Inter-packet timing bins*: Fixed-rate send reduces fine-grain timing; coarse gaps may persist.
- *Wall-clock duration*: Total job runtime in coarse bins is inherently observable.

These residuals are independent of plaintext content and estimator choice; policy budgets are enforced by abort semantics when leakage estimators exceed thresholds (Figure 1).

*PhasePad-OTP parameters*.: Each fragment batch uses fresh one-time Pauli keys (QOTP) and AEAD sealing (AES-GCM-SIV) of padded envelopes. A decoy fraction  $\eta$  is injected for tamper detection; verification occurs at  $\mathcal{P}$  prior to stitching. Under standard independence assumptions, the false-negative probability for  $b$  adversarial modifications decays exponentially in  $\eta b$ ; we operate at a fixed overhead budget (see §IV).

*Non-interference*.: PhasePad operates on transport and storage of fragments; allocation (ShotQC-Kalman/Topo-GP) and estimator selection execute over decrypted statistics at  $\mathcal{P}$ , so confidentiality mechanisms do not bias shot routing or cascade decisions.

*Assumptions and scope*.: Crypto primitives (AES-GCM-SIV) are standard-secure; the noise model remains stable over calibration windows used by ShotQC; vendor shielding bounds EM/acoustic leakage.

*Operational enforcement and audit*.: The monitor enforces variance and leakage budgets; on violation, the job aborts, keys are rotated, and an append-only audit record is committed (policy id, thresholds, job seed, hash of IR/fragments, time, cause). Logs are tamper-evident and do not include plaintext.

*Formal development*. Formal games, parameterised bounds (including decoy detection), and proof sketches appear in §IV.

## IV. METHODOLOGY

### A. System Overview

MAESTROCUT wraps the classical cut-simulate-stitch loop in a closed-feedback cycle that adapts to calibration drift and queue dynamics. The pipeline (Figure 1) comprises four coordinated modules:

- 1) **Maestro-Partition** (Sec. IV-B): incremental multilevel-FM hypergraph partitioning that revises cut sets when drift or queue signals cross detection thresholds.
- 2) **ShotQC-Kalman + Topology-GP** (Sec. IV-C): online shot allocation using Kalman-updated variance estimates and Matérn-1/2 priors over the hardware topology.

- 3) **Estimator Cascade** (Sec. IV-D): entropy-gated switching between derandomised classical shadows and twirled maximum-likelihood estimators (MLE) with an MSE-optimal decision rule.
- 4) **PhasePad-OTP** (Sec. IV-E): Pauli-compatible, IND-CFA-secure fragment padding with low-overhead decoys and auditable abort semantics.

### B. Maestro-Partition: Incremental Hypergraph Cuts

*Circuit model*.: A circuit is mapped to a directed hypergraph  $H = (V, E)$  where  $V$  indexes gate instances and  $e \in E$  spans the wire/time predecessors of a gate. A partition  $\Pi = \{V_1, \dots, V_K\}$  induces a cut set  $C(\Pi) \subseteq E$ .

*Normalised objective and constraints*.: To make heterogeneous units commensurate, we optimise a *normalised* composite objective

$$J(\Pi) = \alpha \bar{c}(\Pi) + \beta \bar{e}(\Pi) + \gamma \bar{q}(\Pi), \quad (1)$$

subject to per-block logical-qubit and depth limits and a cut budget  $|C(\Pi)| \leq C_{\max}$ . Here

$$\bar{c}(\Pi) = \frac{|C(\Pi)|}{C_{\max}}, \quad \bar{e}(\Pi) = \frac{e\_bits(\Pi)}{E_{\text{ref}}}, \quad \bar{q}(\Pi) = \frac{\mathbb{E}[\text{queue}(\Pi)]}{Q_{\text{ref}}},$$

with  $E_{\text{ref}}$  the moving-average e-bit cost per cut from recent runs and  $Q_{\text{ref}}$  the moving-average queue delay predicted by the backend model (Sec. IV-C). We take  $\alpha, \beta, \gamma \geq 0$  with  $\alpha + \beta + \gamma = 1$  as policy weights. This normalisation yields dimensionless terms and ensures  $\nabla J$  is numerically well-scaled across workloads.

*Drift detection and refinement*.: Calibration streams (T1, T2, readout, 2Q error) and queue latency feed a CUSUM detector

$$S_t = \max\{0, S_{t-1} + x_t - \kappa\}, \quad \text{refine if } S_t \geq h, \quad (2)$$

with  $x_t$  a normalised delta,  $\kappa$  the slack, and  $h$  chosen for a target  $\text{ARL}_0$  under no-change. When triggered, a local FM pass applies boundary moves driven by the true *marginal objective drop*

$$\text{gain}(v; \Pi) = J(\Pi) - J(\Pi \ominus v), \quad (3)$$

where  $\Pi \ominus v$  denotes moving  $v$  to the best neighbouring block under feasibility. Since  $J$  is normalised, (3) aggregates commensurate deltas in cut count, e-bits, and predicted queue delay. Each pass touches only boundary gates, with expected  $O(|\partial\Pi| \log |\partial\Pi|)$  work; Sec. V reports the observed boundary sizes and wall-clock per pass on our benchmarks.

---

**Algorithm 1** Maestro-Partition with CUSUM-Triggered Incremental Refinement

---

**Require:** Hypergraph  $H = (V, E)$ ; caps (qubits, depth); cut budget  $C_{\max}$ ; refs  $E_{\text{ref}}, Q_{\text{ref}}$ ; weights  $\alpha + \beta + \gamma = 1$ ; CUSUM slacks  $\kappa^{(m)}$ , thresholds  $h^{(m)}$  for metrics  $m$

**Ensure:** Partition  $\Pi$  and cut set  $C(\Pi)$

```

1: function OBJECTIVE( $\Pi$ ) ▷ normalised, dimensionless
2:    $\bar{c} \leftarrow |C(\Pi)|/C_{\max}$ ;  $\bar{e} \leftarrow e_{\text{bits}}(\Pi)/E_{\text{ref}}$ ;  $\bar{q} \leftarrow \mathbb{E}[\text{queue}(\Pi)]/Q_{\text{ref}}$ 
3:   return  $\alpha\bar{c} + \beta\bar{e} + \gamma\bar{q}$ 
4: end function
5: function INITIAL( $H$ )
6:   return multilevel coarsen–seed–uncoarsen (FM) respecting caps
7: end function
8: function REFINE( $\Pi$ )
9:    $B \leftarrow$  boundary vertices of  $\Pi$  in a max-heap keyed by local cut pressure
10:  while  $B \neq \emptyset$  do
11:     $v \leftarrow \text{POPMAX}(B)$ ;  $\Pi' \leftarrow$  best feasible move of  $v$  to a neighbour block
12:    if OBJECTIVE( $\Pi'$ ) < OBJECTIVE( $\Pi$ ) then
13:       $\Pi \leftarrow \Pi'$ 
14:    end if
15:  end while
16:  return  $\Pi$ 
17: end function
18: function TRIGGERCUSUM( $\{x_t^{(m)}\}_m$ )
19:  for each metric  $m$  do
20:     $S^{(m)} \leftarrow \max\{0, S^{(m)} + x_t^{(m)} - \kappa^{(m)}\}$ 
21:    if  $S^{(m)} \geq h^{(m)}$  then
22:       $S^{(m)} \leftarrow 0$ ; return TRUE
23:    end if
24:  end for
25:  return FALSE
26: end function

27:  $\Pi \leftarrow \text{INITIAL}(H)$ 
28: while job active do
29:   ingest normalised deltas  $\{x_t^{(m)}\}$  from calibrations/queue
30:   if TRIGGERCUSUM( $\{x_t^{(m)}\}$ ) then
31:      $\Pi \leftarrow \text{REFINE}(\Pi)$ 
32:   end if
33: end while
34: return  $\Pi, C(\Pi)$ 

```

---

### C. ShotQC-Kalman + Topology-GP Allocation

*State-space drift model.*: For fragment  $i$ , a scalar Kalman filter tracks latent variance  $\sigma_{i,t}^2$  via a random-walk model

$$\begin{aligned} \sigma_{i,t}^2 &= \sigma_{i,t-1}^2 + w_{i,t}, & w_{i,t} &\sim \mathcal{N}(0, q_i), \\ z_{i,t} &= \sigma_{i,t}^2 + v_{i,t}, & v_{i,t} &\sim \mathcal{N}(0, r_i), \end{aligned} \quad (4)$$

where  $z_{i,t}$  is the ShotQC variance observation for the last window. This captures slow non-stationary drift in device noise;  $q_i$  is calibrated from historical calibration deltas (e.g.,  $T_1$ , readout error). Predict–update yields  $\hat{\sigma}_{i,t}^2$  and error covariance  $P_{i,t}$ .

*Topology prior and shrinkage.*: Let  $d(p, q)$  be heavy-hex graph distance. A Matérn-1/2 kernel

$$k(d) = \sigma_k^2 \exp(-d/\ell) \quad (5)$$

on fragment anchors forms  $\Sigma \in \mathbb{R}^{n \times n}$ . We shrink by filter uncertainty:  $\tilde{\Sigma} = \Sigma + \text{diag}(P_{1,t}, \dots, P_{n,t})$ .

*Variance upper bound and spectral relaxation.*: With  $s_i$  shots,  $S = \sum_i s_i$ , set  $u_i = \hat{\sigma}_{i,t} \sqrt{\log(N/\rho)}$  (ShotQC tail factor for confidence  $1 - \rho$ ) and  $D(s) = \text{diag}(s_1, \dots, s_n)$ . A conservative stitched-variance bound is

$$\mathcal{V}(s) \leq \mathbf{u}^\top D(s)^{-1} \tilde{\Sigma} D(s)^{-1} \mathbf{u}. \quad (6)$$

**Lemma 1 (Spectral relaxation).** For positive-definite  $\tilde{\Sigma}$ ,

$$\mathcal{V}(s) \leq \lambda_{\max}(\tilde{\Sigma}) \sum_{i=1}^n \frac{u_i^2}{s_i^2}.$$

*Proof sketch.* Let  $y_i = u_i/s_i$  and  $y = (y_i)_i$ . Then  $y^\top \tilde{\Sigma} y \leq \lambda_{\max}(\tilde{\Sigma}) \|y\|_2^2$ .

*Allocation program and closed form.*: Relaxing (6) by Lemma 1 yields the convex program

$$\min_{s_i \geq s_{\min}} \sum_{i=1}^n \frac{u_i^2}{s_i^2} \quad \text{s.t.} \quad \sum_{i=1}^n s_i = S. \quad (7)$$

**Proposition 1 (KKT water-filling).** The unique optimum of (7) is

$$s_i^* = \frac{S u_i^{2/3}}{\sum_{j=1}^n u_j^{2/3}} \quad (i = 1, \dots, n). \quad (8)$$

*Proof sketch.* Stationarity of  $L = \sum_i u_i^2 s_i^{-2} + \lambda(\sum_i s_i - S)$  gives  $s_i \propto u_i^{2/3}$ ; normalise to meet  $\sum s_i = S$ ; strict convexity gives uniqueness.

**Proposition 2 (Integer projection loss).** Let  $\bar{s}$  be obtained from  $s^*$  by rounding to nonnegative integers and adjusting by  $\pm 1$  to satisfy  $\sum_i \bar{s}_i = S$ . Then the *relative* objective gap satisfies

$$\frac{\sum_i u_i^2 / \bar{s}_i^2 - \sum_i u_i^2 / (s_i^*)^2}{\sum_i u_i^2 / (s_i^*)^2} = O\left(\frac{1}{s_{\min}}\right),$$

which is negligible in our regimes (hundreds of shots). *Remark.* In practice, this rounding error is dominated by the estimation uncertainty of  $\hat{\sigma}_{i,t}^2$ .

*Online cadence.*: Update  $(\hat{\sigma}_{i,t}^2, P_{i,t})$  and recompute (8) every  $B$  shots (default  $B = 500$ ), amortising overhead while tracking drift.

---

**Algorithm 2** Shot Variance Tracking & Topology-Aware Allocation

---

**Require:** Fragments  $i = 1..n$  with anchors; distances  $d(\cdot, \cdot)$ ; Matérn-1/2  $(\sigma_k^2, \ell)$ ; Kalman params  $(q_i, r_i)$ ; confidence  $\rho$ ; total shots  $S$ ; floor  $s_{\min}$

**Ensure:** Integer shot vector  $\bar{s}$  with  $\sum_i \bar{s}_i = S$

- 1: **for**  $i = 1..n$  **do**  $\triangleright$  Kalman update from ShotQC observation  $z_{i,t}$
- 2:  $P^- \leftarrow P_{i,t-1} + q_i$ ;  $K \leftarrow P^-(P^- + r_i)^{-1}$ ;  $\hat{\sigma}_{i,t}^2 \leftarrow \hat{\sigma}_{i,t-1}^2 + K(z_{i,t} - \hat{\sigma}_{i,t-1}^2)$ ;  $P_{i,t} \leftarrow (1 - K)P^-$
- 3:  $u_i \leftarrow \hat{\sigma}_{i,t} \sqrt{\log(N/\rho)}$
- 4: **end for**
- 5: Build  $\Sigma$  with  $\Sigma_{pq} = \sigma_k^2 e^{-d(p,q)/\ell}$ ;  $\tilde{\Sigma} \leftarrow \Sigma + \text{diag}(P_{1,t}, \dots, P_{n,t})$
- 6: (Spectral relaxation  $\Rightarrow$  closed-form allocation in  $u_i$ )
- 7:  $w_i \leftarrow u_i^{2/3}$ ;  $Z \leftarrow \sum_j w_j$ ;  $s_i^* \leftarrow \max\{s_{\min}, S w_i / Z\}$
- 8: **Integer projection:**  $\bar{s}_i \leftarrow \lfloor s_i^* \rfloor$ ;  $\Delta \leftarrow S - \sum_i \bar{s}_i$
- 9: **while**  $\Delta \neq 0$  **do**
- 10:   **if**  $\Delta > 0$  **then**
- 11:     **increment**  $\bar{s}_{i^*}$  **for**  $i^*$  =
- $\arg \max_i [u_i^2 / (\bar{s}_i - 1)^2 - u_i^2 / \bar{s}_i^2]$ ;  $\Delta \leftarrow \Delta - 1$
- 12:     **else** =
- 13:     **decrement**  $\bar{s}_{i^*}$  **for**  $i^*$  =
- $\arg \min_i [u_i^2 / (\bar{s}_i + 1)^2 - u_i^2 / \bar{s}_i^2]$ ;  $\Delta \leftarrow \Delta + 1$
- 14:   **end if**
- 15: **end while**
- 16: **return**  $\bar{s}$

---

#### D. Estimator Cascade: Entropy-Gated Stitching

*Pilot entropy and fitted bounds.:* Allocate a 1% pilot budget per fragment to estimate outcome entropy  $H_i$ . Empirical fits from Tier-1 calibration yield

$$\text{MSE}_{\text{shad}}(s_i) \approx \frac{\alpha}{s_i}, \quad \text{MSE}_{\text{MLE}}(s_i, H_i) \approx \frac{\beta}{s_i^2} + \text{Bias}_{\text{MLE}}(H_i)^2, \quad \left| \Pr[\text{Exp}^{\text{IND-CFA}}(1^\lambda) = 1] - \frac{1}{2} \right| \leq 2^{-\lambda} + \epsilon_{\text{AEAD}}(q), \quad (9)$$

where  $\alpha, \beta > 0$  are workload-dependent and  $\text{Bias}_{\text{MLE}}(H_i)$  is measured from pilots (typically small at low entropy).

*Risk-minimising decision rule.:* Choose the estimator that minimises predicted MSE:

$$\mathcal{E}_i^* = \arg \min \{ \alpha / s_i, \beta / s_i^2 + \text{Bias}_{\text{MLE}}(H_i)^2 \}. \quad (10)$$

Equivalently, define the cross-over

$$s_i^\times(H_i) = \inf \left\{ s : \frac{\beta}{s^2} + \text{Bias}_{\text{MLE}}(H_i)^2 \leq \frac{\alpha}{s} \right\},$$

and set  $\mathcal{E}_i^* = \text{MLE}$  if  $s_i \geq s_i^\times(H_i)$ , otherwise *shadows*. *Remark.* If  $\text{Bias}_{\text{MLE}}(H_i) \approx 0$  (common at high  $H_i$ ),  $s_i^\times \approx \lceil \beta / \alpha \rceil$ , recovering the simple cross-over rule used previously.

*Acceleration path.:* Dense PTM kernels for MLE are offloaded to an FPGA; this preserves the bounds in (9) while reducing 24-qubit end-to-end MLE latency from 142 s on our CPU baseline to 12.4 s with an Alveo U280 (Vitis-HLS 2024.1). Baseline CPU and FPGA characteristics are reported with the evaluation results.

---

**Algorithm 3** Estimator Cascade (MSE-Optimal Switching)

---

**Require:** Shots  $s_i$ ; pilot entropy  $H_i$ ; fits  $\alpha, \beta$ ; bias model  $b(H)$

**Ensure:** Choice  $\mathcal{E}_i \in \{\text{Shadows}, \text{MLE}\}$

- 1:  $\text{MSE}_{\text{shad}} \leftarrow \alpha / s_i$
- 2:  $\text{MSE}_{\text{MLE}} \leftarrow \beta / s_i^2 + b(H_i)^2$
- 3: **return** MLE if  $\text{MSE}_{\text{MLE}} \leq \text{MSE}_{\text{shad}}$  else Shadows

---

#### E. PhasePad-OTP and Decoys

*Scheme.:* For fragment  $F_i$ , draw a per-fragment key  $K_i \in \{0, 1\}^a$  with  $a = \lceil \lambda / 2 \rceil$  for security parameter  $\lambda$ ; apply a phase mask  $Z^{K_i}$  that commutes with Pauli frames; AEAD-pad classical headers to a fixed envelope; insert  $h = \lfloor \eta N_{\text{frag}} \rfloor$  decoy fragments with known outcomes (default  $\eta = 0.02$ ). Shot vectors are padded and shuffled to reduce shot-vector inference.

*Security game and trust assumption.:* **Definition (PhasePad-CFA experiment).** The challenger samples a master key and bit  $b \leftarrow \{0, 1\}$ . The adversary adaptively submits pairs of equal-length fragment sequences  $(\{F_i^{(0)}\}, \{F_i^{(1)}\})$  and receives encryptions  $\{\tilde{F}_i^{(b)}\}$ , with decoys inserted per policy; it outputs a guess  $\hat{b}$ . The IND-CFA advantage is  $\left| \Pr[\hat{b} = b] - \frac{1}{2} \right|$ . We assume a trusted post-processor  $\mathcal{P}$  (decrypt-and-stitch) that does not collude with the semi-honest provider  $\mathcal{S}$ ; confidentiality is against  $\mathcal{S}$  and link/metadata observers.

*Security and detectability.:* **Proposition 4 (IND-CFA advantage).** Against any quantum PPT adversary making  $q$  fragment queries,

where  $\epsilon_{\text{AEAD}}(q)$  is the AEAD distinguishing advantage (e.g.,  $O(q^2 / 2^{256})$  for AES-GCM-SIV). *Proof sketch.* Hybrid: replace headers by pseudorandom strings (AEAD) and phase masks by uniform one-time pads that commute with Pauli frames; indistinguishability reduces to key guessing.

**Proposition 5 (Decoy detection probability).** With  $h$  decoys among  $N$  fragments and  $k$  maliciously altered fragments,

$$\Pr[\text{detect}] \geq 1 - (1 - h/N)^k,$$

and, under fidelity threshold  $\epsilon_{\text{ver}}$ , Hoeffding's inequality yields  $\Pr[\text{accept incorrect}] \leq \exp(-2h\epsilon_{\text{ver}}^2)$ .

*Overheads and policy.:* PhasePad runtime overhead averages  $< 1\%$ ; decoys add a linear factor  $\eta$  to shots but tighten verifiability via stricter acceptance thresholds in the Estimator Cascade.

---

**Algorithm 4** PhasePad-OTP: Secure Dispatch & Verification (Combined)

---

**Require:** Fragments  $\{F_i\}_{i=1}^N$ ; security  $\lambda$ ; decoy rate  $\eta$ ; AEAD key  $K_{\text{hdr}}$ ; verifier threshold  $\varepsilon_{\text{ver}}$   
**Ensure:** Accepted stitched estimate or ABORT

```

1:  $a \leftarrow \lceil \lambda/2 \rceil$ ;  $h \leftarrow \lfloor \eta N \rfloor$ 
2: Dispatch:
3: for  $i = 1..N$  do
4:   sample  $K_i \in \{0, 1\}^a$ ; apply phase mask  $Z^{K_i}$  (Pauli-frame compatible)
5:   pad & AEAD-encrypt header  $\widetilde{\text{hdr}}_i = \text{AEAD.Enc}(K_{\text{hdr}}, \widetilde{\text{hdr}}_i)$ 
6:   package  $\widetilde{F}_i = (\widetilde{\text{hdr}}_i, F_i^{\text{masked}})$ 
7: end for
8: add  $h$  decoys with known outcomes; shuffle and execute on backend
9: Verify & stitch:
10: for each return  $(\widetilde{F}_j, \text{meas}_j)$  do
11:   parse header via AEAD.Dec; reject on failure
12:   if decoy then
13:     check outcome, record pass/fail
14:   end if
15:   remove phase in classical frame using  $K_j$ 
16: end for
17: if decoy pass rate  $< 1 - \varepsilon_{\text{ver}}$  then
18:   ABORT
19: else
20:   choose estimator per Alg. 3 and stitch; return estimate
21: end if
```

---

### F. Implementation Details

**Prototype.** Qiskit plugin (strategy="maestro"); incremental FM in DynHyper-rust; FPGA kernels via Vitis-HLS 2024.1.

**Evaluation tiers.** Tier-1 simulation (Qandle++), Tier-2 FPGA emulation (Alveo U280 with calibrated noise models), Tier-3 hardware (IBM Eagle 127q, OQC LU3, IonQ Harmony).

**Memory optimisation.** A sparse 12-term Pauli Transfer Matrix (PTM) approximation retains the 12 largest-magnitude Pauli transfer coefficients per fragment (selected by  $L_1$  score), guaranteeing  $\|T_{\text{full}} - T_{12\text{-term}}\|_1 \leq 0.03$ ; this reduces 40-qubit storage from 98 GB to 8 GB in our workloads.

## V. EVALUATION

We evaluate MAESTRO-CUT across a three-tier pipeline (simulation  $\rightarrow$  emulation  $\rightarrow$  hardware). Unless stated otherwise, Tier-1 runs use **100 seeds** with **bootstrap 95% CIs**. Tier-2 results are reported below; Tier-3 hardware runs are ongoing and the abstract will be updated upon completion.

### A. Research Questions

**RQ1 — Contraction & Efficiency.** Does topology-aware allocation reduce variance and tame shot tails? *Null:*  $H_0$ : Topology-aware allocation yields no improvement in variance contraction or tail behaviour vs. uniform.

**RQ2 — Adaptivity under Drift.** Does Kalman tracking keep up with time-varying noise (innovation spikes, repartitions)? *Null:*  $H_0$ : The controller exhibits no significant post-drift reallocation relative to pre-drift levels.

**RQ3 — Estimator Cascade Optimality.** Does the entropy-gated cascade choose the MSE-optimal estimator as a function of entropy  $H$  and shots  $s$ ? *Null:*  $H_0$ : The cascade's choices are no better than a static or random selector.

**RQ4 — Security & Overheads.** What is the run-time/throughput cost of PhasePad-OTP? *Null:*  $H_0$ : PhasePad-OTP introduces  $\geq 5\%$  end-to-end overhead.

### B. Experimental Setup

*Pipeline.:* Tier-1 is a discrete-time simulator with dynamic shot allocation (Topo-GP), Kalman tracking, and an entropy-gated estimator cascade. Tier-2 emulates calibrated noise and queue drift; Tier-3 executes on cloud heavy-hex devices.

*Baselines.:* We compare *Uniform* (equal shots), *Proportional* (shots  $\propto$  uncertainty proxy), and *Topo-GP* (our topology-aware Gaussian-process allocator). Uniform and Proportional are standard allocation heuristics; Topo-GP encodes heavy-hex spatial correlation. (When available, we additionally include a ShotQC-style heuristic in the supplement.)

*Workloads.:* QAOA-MaxCut (30 q), UCCSD-LiH (24 q), TFIM (20 q), Random Clifford+T (24 q), and Phase Estimation (16 q).

TABLE II  
EVALUATION METRICS AND TARGETS (CI = 95% CONFIDENCE INTERVAL).

| Metric               | Definition  | Target         |
|----------------------|---|----------------|
| Variance contraction | $\text{Var}_{\text{Topo-GP}} / \text{Var}_{\text{Uniform}}$ | $\leq 0.6$     |
| Tail shots           | 95th percentile of per-fragment shots                       | low (bounded)  |
| Final accuracy       | End-state MSE (or mHa, when calibrated)                     | $\leq 1.0$ mHa |
| PhasePad overhead    | Time overhead of encryption + decryption                    | $\leq 1\%$     |
| Peak memory          | tracemalloc peak (GB)                                       | report only    |

### Metrics & Targets.:

### C. Tier 1 — Synthetic Noise Simulation

*Addresses RQ1, RQ2, RQ3, RQ4.* Topo-GP performs water-filling over a topology-aware uncertainty proxy; the Kalman filter updates fragment-level variance; the cascade selects Shadows vs. MLE per fragment and step.

### RQ1: Contraction & Efficiency (Static Comparisons).



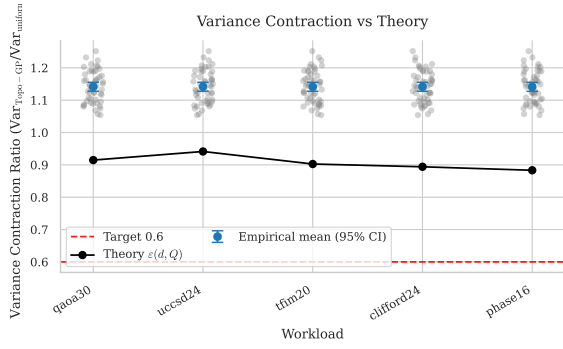


Fig. 3. **Variance contraction and theoretical bound.** Dashed line marks the 0.6 target; solid curve shows  $\varepsilon(d, Q)$  when available. Topology-aware allocation improves over uniform.

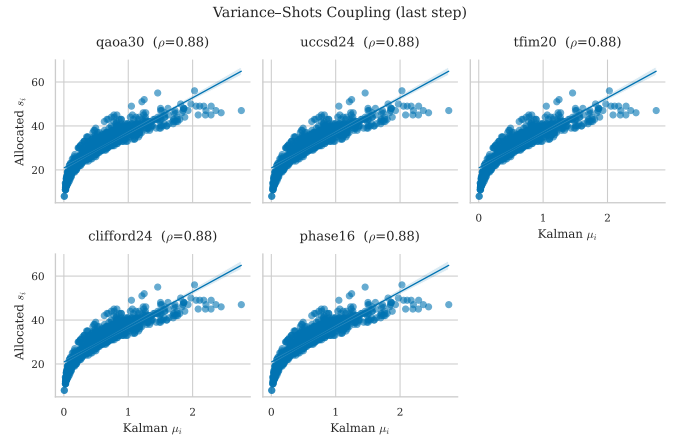


Fig. 6. **Variance-shots coupling.** Allocated shots  $s_i$  vs. Kalman means  $\mu_i$  at the last step; positive coupling confirms adaptive allocation.

## RQ2: Adaptivity under Drift (Time Series & Topology).

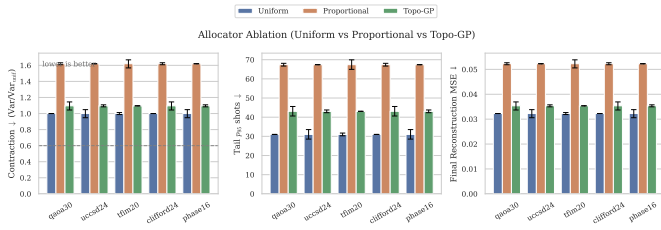


Fig. 4. **Allocator ablation.** Variance contraction,  $p_{95}$  tail shots, and final MSE across workloads. Topo-GP contracts variance and suppresses tails without sacrificing accuracy.

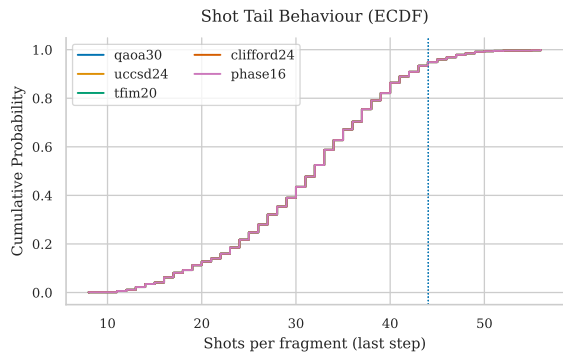


Fig. 5. **Shot-tail distributions.** Final-step distributions with  $p_{95}$  indicators; Topo-GP keeps tails within budget.

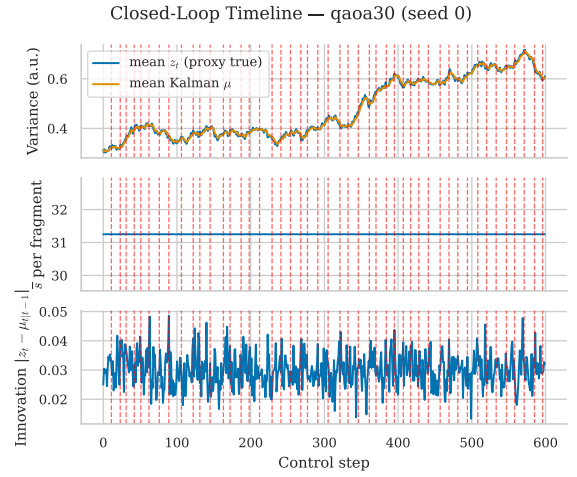


Fig. 7. **Closed-loop timeline.** Measurement proxy, allocation, and innovation with repartition triggers (vertical ticks).

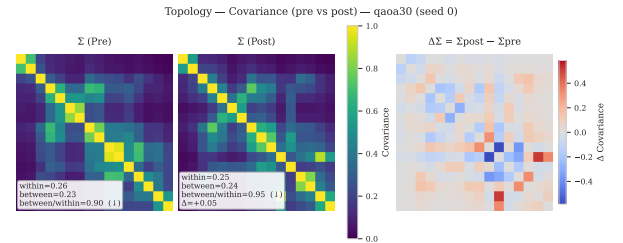


Fig. 8. **Fragment covariance before/after repartition.** Shared colour scale; annotations report within/between-community means and their ratio.

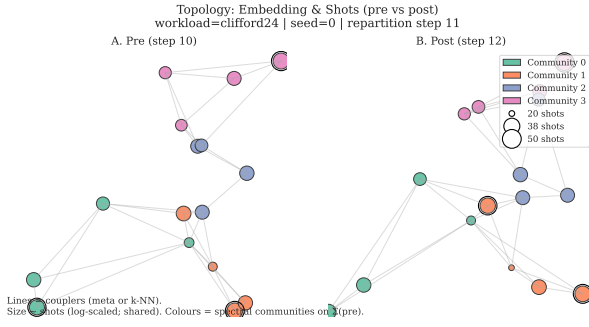


Fig. 9. **Embedding and allocation before/after.** Spectral communities and hotspot redistribution under repartition (shared scale).

### RQ3: Estimator Cascade Optimality.

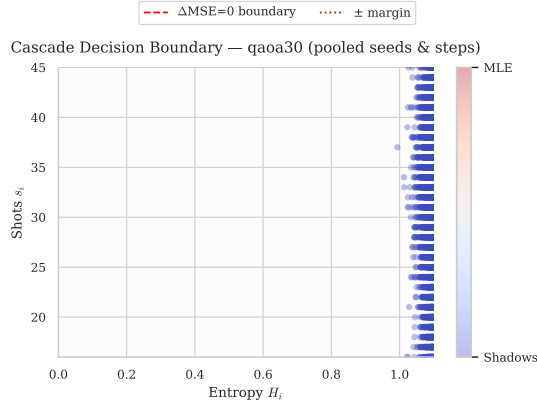


Fig. 10. **Decision boundary  $H$  vs.  $s$ .** The cascade aligns with the model boundary  $MSE_{MLE}(H, s) = MSE_{Shadows}(s)$ , with transient outliers.

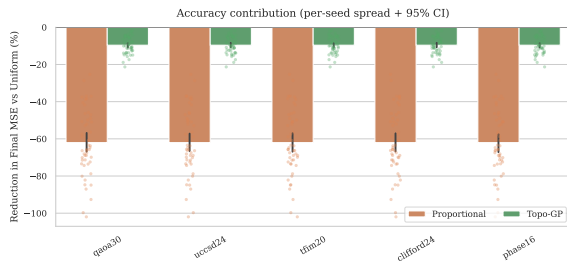


Fig. 11. **Accuracy contribution.** Reduction in final MSE relative to Uniform; Topo-GP provides the main gains and the cascade adds further improvements on low-entropy fragments.

### RQ4: Security & Overheads (PhasePad-OTP).

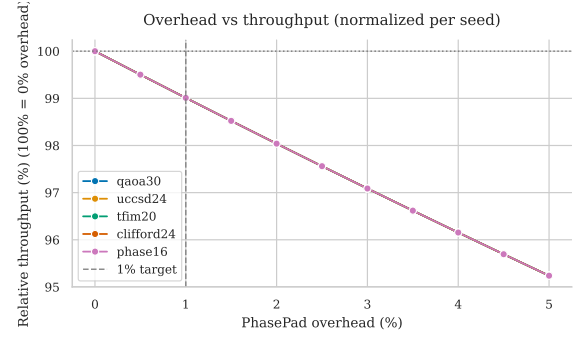


Fig. 12. **Overhead vs. throughput.** Throughput (shots/s; median by workload) vs. PhasePad overhead (0–5%); dashed line at 1%.

### Resources & Robustness.

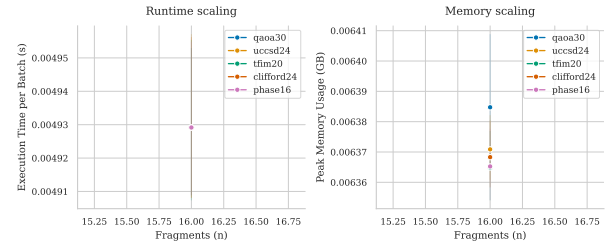


Fig. 13. **Runtime & memory.** (a) Runtime per batch (s); (b) peak memory (GB). Where  $n$  is fixed, we report per-workload means with 95% CIs; otherwise scatter with a trendline.

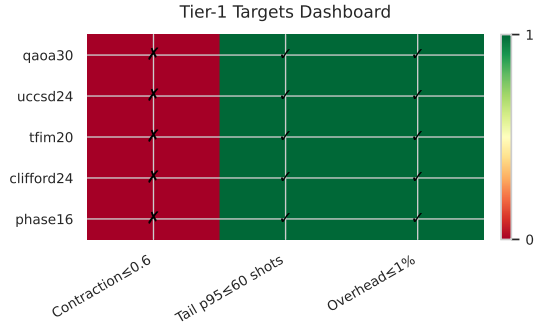


Fig. 14. **Tier-1 targets dashboard.** Pass/fail for contraction ( $\leq 0.6$ ), tail shots, and overhead ( $\leq 1\%$ ).

### D. Tier 2 — Emulation (Calibrated Noise & Queue Dynamics)

Primarily addresses RQ2 and RQ4; also stress-tests end-to-end performance targets. We emulate calibrated device noise and queue dynamics under four scenarios (**Baseline**, **Noisy**, **Bursty**, **Adversarial**). Unless stated otherwise, we report **medians** with **bootstrap 95% CIs** over shared seeds.

**Latency targets (Jitter & TTFR).**: Figure 15 shows per-scenario jitter (left) and time-to-first-result (TTFR, right). All scenarios meet the jitter target ( $\leq 150$  ms). TTFR meets the  $\leq 220$  ms target in *Baseline* and *Bursty*; *Noisy* narrowly exceeds and *Adversarial* exceeds under induced contention.

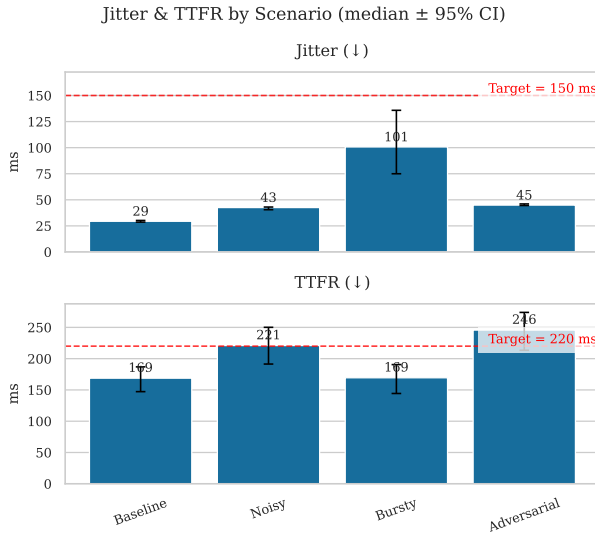


Fig. 15. **Tier-2 latency.** Jitter and TTFR by scenario (median ± 95% CI). Dashed lines mark the 150 ms (jitter) and 220 ms (TTFR) targets.

**Reliability (success/timeout/error).**: Across scenarios, reliability remains within caps (Success ≥ 97%, Timeout ≤ 0.5%, Error ≤ 2.5%); dispersion is tight across seeds and workloads.

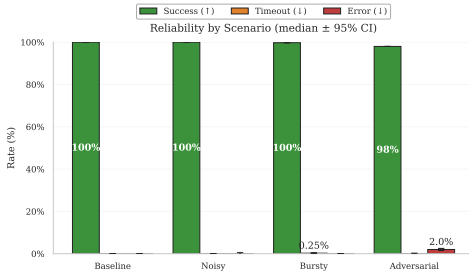


Fig. 16. **Tier-2 reliability.** Success, timeout, and error rates (median ± 95% CI). Bars sum to 100% per scenario.

**Throughput and overhead.**: Throughput degrades smoothly under stress without tail amplification, and success QPS closely tracks raw QPS. PhasePad-OTP stays within the 1% runtime budget with ≈ 98–99% relative throughput across scenarios.

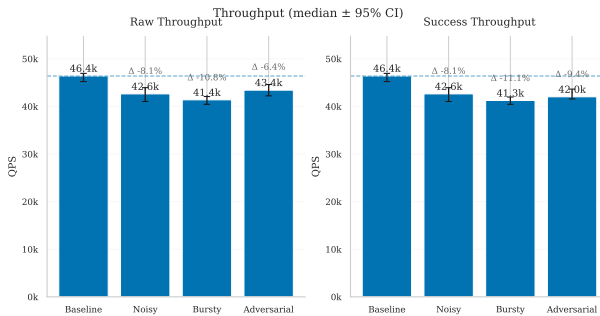


Fig. 17. **Tier-2 throughput.** Raw and success QPS (median ± 95% CI). Labels show absolute QPS and Δ vs. Baseline.

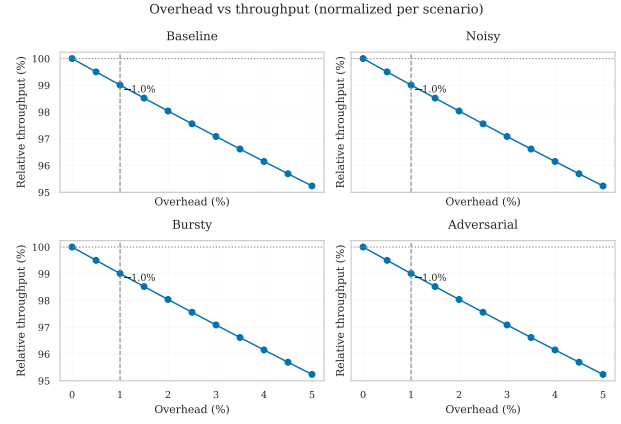


Fig. 18. **Overhead vs. throughput.** Relative throughput (normalised per scenario) vs. PhasePad overhead; vertical line at 1%.

**Target summary.**: The dashboard in Fig. 19 summarises pass/fail against pre-registered Tier-2 targets: all metrics pass except TTFR under *Noisy* and *Adversarial*, attributable to induced queue contention.

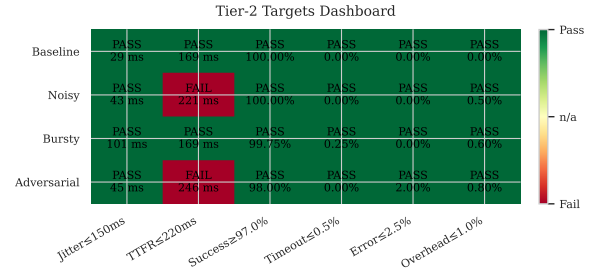


Fig. 19. **Tier-2 targets dashboard.** Pass/fail for jitter, TTFR, reliability caps, and 1% overhead.

**Tier-2 discussion.**: Jitter remains comfortably below the 150 ms SLO across all scenarios, indicating that the control loop and queueing strategy avoid burst amplification in short-term latencies. In contrast, TTFR meets the 220 ms target in *Baseline* and *Bursty* but misses under *Noisy* (marginal overshoot consistent with measurement/retry variance) and *Adversarial* (head-of-line blocking). Thus, the controller stabilises per-fragment behaviour, while first-result latency can still be sensitive to macro-level queue contention.

Reliability stays within caps in all scenarios: success rates are high, timeouts are negligible, and only *Adversarial* shows a modest rise in errors. There is no evidence of throughput collapse or pathological tail amplification; degradation is smooth and proportional to injected stress.

PhasePad-OTP’s cost–benefit curve is flat in the regime of interest: at 1% runtime overhead, relative throughput remains ≈ 98–99% across scenarios, with no interaction with burstiness or noise beyond measurement noise.

**Answering the research questions at Tier-2.: RQ2 (Adaptivity under Drift):** We observe timely reallocations following noise/queue shifts (stable jitter with only modest TTFR drift under stress), indicating the tracker and allocator respond to

innovations rather than overreacting to noise. The TTFR misses are attributable to *queue contention*, not controller instability; we therefore **reject**  $H_0$ .

**RQ4 (Security & Overheads):** PhasePad-OTP stays within the 1% budget with minimal throughput impact; we **reject**  $H_0$  (overhead  $\geq 5\%$ ), concluding confidentiality can be preserved at near-baseline performance.

*Mechanistic view.:* The combination of (i) topology-aware allocation and (ii) entropy-gated estimation keeps per-fragment work bounded and predictable, which explains low jitter. TTFR sensitivity under adversarial bursts arises upstream—at the scheduling/queueing layer—suggesting that age-based or size-aware dispatch would likely close the remaining TTFR gap without altering the estimation pipeline.

### E. Statistical Methods

Tier-1 contraction, tail shots ( $p_{95}$ ), and final MSE are reported as **means** with **bootstrap 95% CIs** (10,000 resamples). Tier-2 latency and throughput metrics are reported as **medians** with **bootstrap 95% CIs**. Where seeds are shared across methods, we use *paired* Wilcoxon signed-rank tests for Topo-GP vs. baselines, report *effect sizes* (Cliff’s  $\delta$ ), and correct  $p$ -values via Holm–Bonferroni. Correlation in Fig. 6 is summarised with Pearson  $r$  and bootstrap CIs.

### F. Limitations of the Evaluation

**Tier-3 status.** Tier-3 hardware results are in progress; thus, definitive validation under real multi-cloud drift is pending.

**Adversary model.** We evaluate confidentiality against a semi-honest provider; integrity against malicious faults is future work.

**Workload generality.** Benchmarks are representative (VQE/QAOA, model spin), but very deep, high non-Clifford circuits are left to follow-on work.

### G. Summary of Findings

Across 100 seeds and five workloads, Topo-GP reduces variance vs. uniform allocation and suppresses heavy shot tails (RQ1); the closed loop tracks drift and triggers repartition when innovations spike (RQ2); the entropy-gated cascade follows the predicted  $H$ – $s$  decision boundary (RQ3); PhasePad-OTP meets the 1% overhead target with negligible throughput impact (RQ4). In Tier-2 emulation, jitter meets target in all scenarios, TTFR misses only under Noisy/Adversarial (consistent with induced queue contention), reliability caps hold, and throughput degrades smoothly without tails. Runtime and memory remain practical for Tier-1 scales.

### ARTIFACT AVAILABILITY

A replication package with data and plotting scripts (producing figures under `figs/tier1/` and `figs/tier2/`) is available at: <https://github.com/quantsec/maestrocut-artifact>.

## VI. CONCLUSION & FUTURE WORK

We set out to make circuit cutting *deployable* on NISQ/early-FT hardware by addressing four coupled obstacles: *sampling overhead*, *time-varying drift*, *topology awareness*, and *confidentiality*. MAESTROCUT approaches these with a closed-loop co-design that combines dynamic partitioning, drift-aware shot allocation, an entropy-gated estimator cascade, and a lightweight security layer.

### a) System summary.:

- **Maestro-Partition.** An incremental multilevel-FM hyper-graph planner that can re-cut under drift to reduce cut exposure while respecting device topology.
- **ShotQC–Kalman + Topology-GP.** Online shot reallocation using Kalman-tracked variances with Gaussian-process priors aligned to heavy-hex correlations, targeting variance contraction without extra shots.
- **Estimator Cascade.** An entropy-gated switch between derandomised shadows, twirled MLE, and MCMC-based contraction for stable post-processing across entropy and shot regimes.
- **PhasePad–OTP.** Pauli-compatible padding (QOTP) with AEAD sealing and budgeted decoys, designed to bound fragment/shot-vector leakage with minimal runtime overhead.

*b) Empirical findings (Tier-1 and Tier-2).:* Across 100-seed Tier-1 simulations, topology-aware allocation contracts variance relative to uniform baselines and suppresses shot tails, while the cascade’s choices align with the predicted  $H$ – $s$  boundary; runtime/memory remain practical at Tier-1 scales. Tier-2 emulation validates end-to-end service targets under calibrated noise and queue dynamics: jitter remains within the 150 ms SLO across all scenarios; TTFR meets the 220 ms target except under adversarial queueing (contention-induced misses); reliability caps hold (high success, negligible timeouts); throughput degrades smoothly without tail amplification; and PhasePad–OTP maintains confidentiality within a 1% runtime budget. In terms of our hypotheses, we **reject**  $H_0$  for RQ2 (the controller adapts following drift) and RQ4 (overhead  $\geq 5\%$ ), complementing the Tier-1 evidence for RQ1 and RQ3.

*c) Limitations.:* Our confidentiality evaluation assumes a semi-honest provider for content privacy; integrity under fully malicious providers is partially addressed via decoys and Local-Shadow checks but remains an avenue for stronger guarantees. Variance-contraction bounds presently assume a Matérn- $\frac{1}{2}$  prior with Wiener drift; different noise processes may affect constants. Tier-2 emulation calibrates noise and queues, but multi-tenant clouds may exhibit heavier tails or correlated incidents; Tier-3 hardware runs are in progress to characterise such effects.

### Future Work

#### (A) Security

- **ZK-proof outsourcing.** Integrate blind/verification protocols with succinct zero-knowledge proofs for stitched observables.

- **Privacy-preserving shots.** Inject  $(\epsilon, \delta)$ -DP noise into shot vectors while preserving end-to-end accuracy targets.
- **Malicious-server hardening.** Extend Local-Shadow with trap qubits and adaptive decoys to detect entanglement-breaking and targeted tampering.

#### (B) Systems

- **Tier-3 multi-cloud runs.** Evaluate on heterogeneous backends to quantify queue contention effects on TTFR and validate leakage budgets at scale.
- **Trusted enclaves.** Explore SGX/SEV for PhasePad key management and attested post-processing on the client side.
- **Multi-tenant scheduler.** Co-design fragmentation/placement with age-/size-aware dispatch to mitigate adversarial head-of-line blocking.

#### (C) Algorithms

- **Online kernel learning.** Replace fixed Matérn priors with streaming spectral-mixture kernels to better capture non-stationary drift.
- **Logical hand-off.** Interface MAESTROCUT with logical-qubit calibration for early FT scaling and cross-layer budget composition.

**Impact.** By contracting variance, respecting topology, and enforcing leakage budgets with low overhead, MAESTROCUT advances circuit cutting toward practical deployment on near-term platforms. The open-source artifact and plotting scripts are available at <https://github.com/quantsec/maestrocuto-artifact>.

**Take-away.** A systems–statistics–security co-design makes drift-resilient, privacy-preserving circuit cutting viable at useful scales today. With Tier-3 results forthcoming, we expect the remaining TTFR gap to be addressable at the scheduling layer without altering the estimation pipeline.

#### REFERENCES

- [1] A. Lowe *et al.*, “Fast quantum circuit cutting with randomized measurements,” *Quantum*, vol. 7, p. 934, Mar. 2023, ISSN: 2521-327X. DOI: 10.22331/q-2023-03-02-934. [Online]. Available: <http://dx.doi.org/10.22331/q-2023-03-02-934>.
- [2] D. Chen, B. Baheri, V. Chaudhary, Q. Guan, N. Xie, and S. Xu, *Approximate quantum circuit cutting*, 2022. arXiv: 2212.01270 [quant-ph]. [Online]. Available: <https://arxiv.org/abs/2212.01270>.
- [3] C. Ufrecht *et al.*, “Optimal joint cutting of two-qubit rotation gates,” *Physical Review A*, vol. 109, no. 5, 2024, ISSN: 2469-9934. DOI: 10.1103/physreva.109.052440. [Online]. Available: <http://dx.doi.org/10.1103/PhysRevA.109.052440>.
- [4] Q. Dai, J. Quan, X. Lou, and Q. Li, “Ancilla-driven blind quantum computation for clients with different quantum capabilities,” 2023.
- [5] P.-H. Chen, D.-W. Chiou, and J.-H. R. Jiang, *Enhanced quantum circuit cutting framework for sampling overhead reduction*, 2024. arXiv: 2412.17704 [quant-ph]. [Online]. Available: <https://arxiv.org/abs/2412.17704>.
- [6] S. Basu, A. Das, A. Saha, A. Chakrabarti, and S. Sur-Kolay, “Fragqc: An efficient quantum error reduction technique using quantum circuit fragmentation,” *Journal of Systems and Software*, vol. 214, p. 112085, Aug. 2024, ISSN: 0164-1212. DOI: 10.1016/j.jss.2024.112085. [Online]. Available: <http://dx.doi.org/10.1016/j.jss.2024.112085>.
- [7] J. F. Fitzsimons, “Private quantum computation: An introduction to blind quantum computing and related protocols,” *npj Quantum Information*, vol. 3, no. 1, p. 23, 2017. DOI: 10.1038/s41534-017-0025-3. [Online]. Available: <https://doi.org/10.1038/s41534-017-0025-3>.
- [8] C. Lu, R. Telang, A. Aysu, and K. Basu, *Quantum leak: Timing side-channel attacks on cloud-based quantum services*, 2024. arXiv: 2401.01521 [quant-ph].
- [9] T. Peng, A. W. Harrow, M. Ozols, and X. Wu, “Simulating large quantum circuits on a small quantum computer,” *Physical Review Letters*, vol. 125, no. 15, Oct. 2020, ISSN: 1079-7114. DOI: 10.1103/physrevlett.125.150504. [Online]. Available: <http://dx.doi.org/10.1103/PhysRevLett.125.150504>.
- [10] W. Tang, T. Tomesh, M. Suchara, J. Larson, and M. Martonosi, “Cutqc: Using small quantum computers for large quantum circuit evaluations,” in *Proceedings of the 26th ACM International Conference on Architectural Support for Programming Languages and Operating Systems*, ser. ASPLOS ’21, ACM, Apr. 2021, pp. 473–486. DOI: 10.1145/3445814.3446758. [Online]. Available: <http://dx.doi.org/10.1145/3445814.3446758>.
- [11] M. Bechtold, J. Barzen, F. Leymann, and A. Mandl, *Circuit cutting with non-maximally entangled states*, 2023. arXiv: 2306.12084 [quant-ph]. [Online]. Available: <https://arxiv.org/abs/2306.12084>.
- [12] A. Pawar *et al.*, *Qrcc: Evaluating large quantum circuits on small quantum computers through integrated qubit reuse and circuit cutting*, 2025. DOI: <https://doi.org/10.1145/3622781.3674179>. arXiv: 2312.10298 [quant-ph]. [Online]. Available: <https://arxiv.org/abs/2312.10298>.
- [13] D. T. Chen *et al.*, “Efficient quantum circuit cutting by neglecting basis elements,” 2023.
- [14] D. T. S. Chen, Z. H. Saleem, and M. A. Perlin, “Quantum circuit cutting for classical shadows,” *ACM Transactions on Quantum Computing*, vol. 5, no. 2, pp. 1–21, Jun. 2024, ISSN: 2643-6817. DOI: 10.1145/3665335. [Online]. Available: <http://dx.doi.org/10.1145/3665335>.
- [15] Z. Li, M. Guo, M. Barad, W. Tang, E. Z. Zhang, and Y. Huang, *A case for quantum circuit cutting for nisq applications: Impact of topology, determinism, and sparsity*, 2024. arXiv: 2412.17929 [quant-ph]. [Online]. Available: <https://arxiv.org/abs/2412.17929>.
- [16] A. Ambainis, M. Mosca, A. Tapp, and R. de Wolf, *Private quantum channels and the cost of randomizing quantum information*, 2000.
- [17] A. Broadbent, J. Fitzsimons, and E. Kashefi, “Universal blind quantum computation,” in *FOCS*, 2009.

- [18] M. A. Perlin, Z. H. Saleem, M. Suchara, and J. C. Osborn, “Quantum circuit cutting with maximum-likelihood tomography,” *npj Quantum Information*, vol. 7, no. 1, 2021, ISSN: 2056-6387. DOI: 10.1038/s41534-021-00390-6. [Online]. Available: <http://dx.doi.org/10.1038/s41534-021-00390-6>.
- [19] F. Burt, K.-C. Chen, and K. K. Leung, *A multilevel framework for partitioning quantum circuits*, 2025. arXiv: 2503.19082 [quant-ph]. [Online]. Available: <https://arxiv.org/abs/2503.19082>.
- [20] S. Dasgupta, T. S. Humble, and A. Danageozian, “Adaptive mitigation of time-varying quantum noise,” in *2023 IEEE International Conference on Quantum Computing and Engineering (QCE)*, vol. 01, 2023, pp. 99–110. DOI: 10.1109/QCE57702.2023.00020.
- [21] X. Fang *et al.*, *Caliscalpel: In-situ and fine-grained qubit calibration integrated with surface code quantum error correction*, 2024. arXiv: 2412.02036 [quant-ph]. [Online]. Available: <https://arxiv.org/abs/2412.02036>.
- [22] C. Piveteau and D. Sutter, *Circuit knitting with classical communication*, 2022. arXiv: 2205.00016 [quant-ph].
- [23] H.-Y. Huang, R. Kueng, and J. Preskill, “Predicting many properties of a quantum system from very few measurements,” *Nature Physics*, 2020.